2008 IEEE International Conference on
Robotics and Automation
Pasadena, CA, USA, May 19-23, 2008

# A Low-cost Motion Tracker and Its Error Analysis

Wei Dong, Kwang Yong Lim, Young Koon Goh, Kim Doang Nguyen,
I-Ming Chen, Song Huat Yeo, Been-Lirn Duh

*Abstract*—**This paper develops a physical model of an inertial/magnetic measurement unit by effectively integrating an accelerometer, a magnetometer, and two gyroscopes for low-g motion tracking applications. The proposed model breaks down the errors contributed by individual components, then determines error elimination methods based on sensor behavior and characteristics, and finally constructs a feedback loop for continuous self-calibration. Measurement errors are reduced by adopting a systematic design methodology: 1) tilt errors are minimized through a careful selection of A/D convertor resolution and by making compensation on sensor bias and scale factor; 2) heading errors are reduced by cancelling out nearby ferrous distortions and making tilt-compensation on the magnetometer; 3) errors from gyroscope measurements are eliminated via the least squares algorithm and continuous corrections using orientation data at the steady-state position. Preliminary tests for low-g motion sensing show that the motion tracker can achieve less than ±0.5° accuracy in tilt and less than ±1° accuracy in yaw angle measurement with above-mentioned methods.**

## I. Introduction

SEVERAL motion capture technologies have been proposed in the last few decades. They can be briefly categorized into: optical, image-based, mechanical, magnetic, inertial, acoustic, and hybrid systems. Among them, inertial measurement units built with micromachined accelerometers and/or rate gyroscopes not only have size and cost advantages, but also offer relatively impressive performance in motion capture applications. Therefore, inertial trackers appear to be the most promising one of all the available technologies in terms of tiny, self-contained, complete, accurate, fast, immune to occlusions, robust, tenacious, wireless, and cheap [1].

However, the uses of inertial motion capture systems are still restricted because electronic offsets and drifts yield significant tracking errors during the integration of linear acceleration and angular rate [2], [3]. More importantly, inertial trackers alone cannot recover reliably from these errors without introducing external reference information. Various technologies including cycle-cancelling algorithm, time-frequency analysis, and filter algorithms were applied to eliminate the impact of offsets and drifts [4]–[6]. But they also increase computational cost and therefore, end up with a complex system that requires more hardware and software resources.

Motion tracking based on sensor fusion of accelerometers, magnetometers, and gyroscopes [7]–[9] represents a promising stand-alone technology in that orientations can be measured solely relying upon gravitational and geomagnetic fields which constitute an absolute coordinate frame of reference. Bachmann *et al.* [7], [8] first introduced such a device and developed a quaternion attitude filter for three-degrees-of-freedom (DOF) orientation tracking of rigid bodies. Zhu *et al.* [9] modeled human body motion with a geometric representation and tracked articulated human motion with inertial/magnetic sensors.

For many low-g (<±2g) applications, such as indoor robot navigation, motion tracking for animation and entertainment, etc., the signal-to-noise ratio is low and thus any unmodeled error in the system would determine the effectiveness of the intended application over time [10]. Unfortunately, compared with a lot of efforts aforementioned on filtering and modeling technologies, not much research has been done to break down the errors contributed by individual sensor components in an inertial/magnetic tracker and to determine what level of signal processing is required.

The objective of this paper is to develop a physical model to effectively integrate the microelectromechanical system-based (MEMS-based) accelerometer, magnetometer, and gyroscopes, in terms of the common parameters published in their manufactures' datasheets. A prototype targeting at ±1° accuracy in orientation measurement (roll/pitch/yaw angles) for low-g motion sensing is realized using commercially available sensors. Calibration and error cancelling methods are discussed based on the understating of the characteristics of individual components and the interactions between them. Preliminary testing of the inertial/magnetic tracker is performed to verify the design concept and error correction methods as well.

## II. Hardware Design

Figure 1 shows the complementary filter approach to the inertial/magnetic measurement unit. Each motion tracker contains three orthogonal accelerometers, three orthogonal magnetometers, and three orthogonal gyroscopes. Tilt angles

Manuscript received September 14, 2007. This work was supported by the Singapore Agency for Science, Technology and Research under the Embedded Hybrid Systems II program.

Wei Dong, Kwang Yong Lim, Young Koon Goh, Kim Doang Nguyen, I-Ming Chen, and Song Huat Yeo are with the Robotics Research Centre, School of Mechanical and Aerospace Engineering, Nanyang Technological University, 50 Nanyang Avenue, Singapore, 639798 (phone: 65-6790-5568; fax: 65-6793-5921; e-mail: wei.dong@alum.mit.edu).

Been-Lirn Duh is with the Interactive and Digital Media Institute, Department of Electrical and Computer Engineering, National University of Singapore, 4 Engineering Drive 3, Singapore, 117576 (e-mail: eledbl@nus.edu.sg).

are calculated from the earth's gravitational vector that is directly measured by a tri-axis accelerometer [11]. Together with the tilt-compensated heading, outputs from the accelerometer and magnetometer are able to yield the steady-state orientation of a rigid body in the form of roll, pitch, and yaw angles. Integration of the angular velocity data from rate gyroscopes also provides the orientation of a body segment in dynamic motions. Errors caused by drifts and scale factor of gyroscopes can be continuously corrected by comparing the difference between the calculation and integration results.

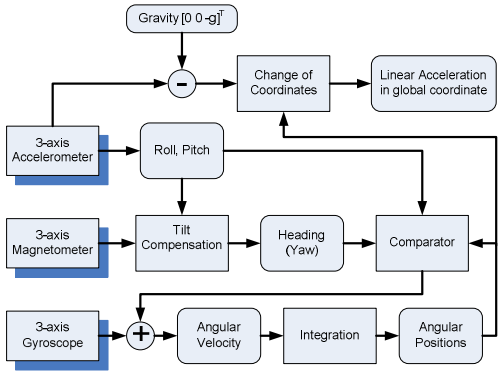


Fig. 1. Complementary filter approach to the inertial/magnetic tracker.

The accelerometer used in the physical model is a tri-axis low-g MEMS-based capacitive accelerometer from STMicroelectronics (LIS3LV02DQ). This sensor measures 7 mm × 7 mm × 1.8 mm, weighs about 0.2 gram, and has an effective sensing range of ±2g/±6g. It includes a sensing element capable of measuring linear acceleration signals over a bandwidth of 640 Hz and an IC interface able to send out the data in 12/16 bit data representation through an Inter-Integrated Circuit/Serial Peripheral Interface (I2C/SPI) serial interface. An alternative is Freescale Semiconductor's MMA7260Q, which has similar performance but only analog outputs.

The magnetometer used here is PNI's MicroMag3, an integrated tri-axis magnetic field sensing module based on Magneto-Inductive (MI) sensors. The module is chosen because it has small size (25.4 mm × 25.4 mm × 19 mm), low power consumption (<500 μA at 3 VDC), large measurement range (±11 Gauss) with high resolution ($1.5 \times 10^{-4}$ Gauss), digital SPI interface, fast sample rate (2000 Hz), stable outputs over temperature, and inherently free from offset drift. An alternative is to construct a magnetometer by interfacing IC and three MI or Magneto-Resistive (MR) sensors mounted orthogonally.

The angular rate sensors selected for the prototype are the yaw rate gyroscope ADXRS300 from Analog Devices and the dual-axis gyroscope IDG-300 from InvenSense. The authors believe they are the smallest gyroscopes currently available in the market: The ADXRS300's size is 7 mm × 7 mm × 3mm and its weight is less than 0.5 gram. The IDG-300 has two sensor elements in a 6 mm × 6 mm × 1.5 mm QFN package. The manufacturers specified maximum allowable angular rates are ±300º/s in yaw, ±500º/s in roll and pitch. These ranges are sufficient to most human body motion tracking applications. The outputs of these gyroscopes are regulated voltages proportional to angular rates.

The design Micro Controller Unit (MCU) is ATMEL's ATmega168, a low-power CMOS 8-bit microcontroller based on the AVR enhanced RISC architecture. In the prototype, it communicates with the accelerometer and magnetometer via the SPI protocol and also functions as a 10-bit A/D convertor (ADC) for gyroscopes. Besides signal processing, the MCU package orientation information with a tracker identification number and then, send it out to the Two Wire Interface (TWI) bus.

Figure 2 depicts the prototype of the inertial/magnetic motion tracker. Each tracker consists of an accelerometer, a magnetometer, a MCU, and two gyroscope modules stacked vertically. All electronic components are running on a 3.3V power. As each individual chip costs less than $20, we are able to achieve a target price of around $100.

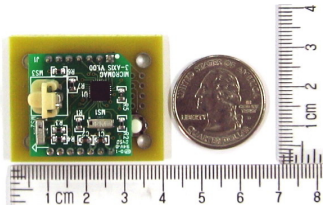


Fig. 2. Prototype of the inertial/magnetic tracker.

## III. ORIENTATION DETERMINATION

Two coordinate frames (see Fig. 3) need to be defined to compute the orientation of the motion tracker:

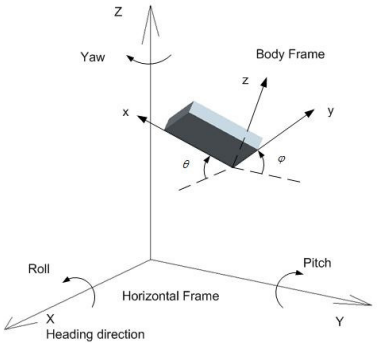


Fig. 3. Coordinate frames (body frame and horizontal frame).

1) *Body Frame* ($x_{body}$ $y_{body}$ $z_{body}$): This frame has its origin at the inertial/magnetic sensor; and each axis points along the sensitive axis of the sensor, respectively. It is a body fixed frame moving together with the body segment where the sensor unit is mounted. It is regarded as a local coordinate in all calculations.

2) *Horizontal Frame* ($X_{hor}$ $Y_{hor}$ $Z_{hor}$): This frame is attached to a horizontal plane normal to the earth's gravity vector. It is a fixed global coordinate. Three axis are arranged in a right handed helix. The negative direction of gravity is defined as the positive direction of $Z_{hor}$.

An accelerometer in its steady state can be directly used to measure the gravity vector g which is always vertical to the horizontal plane. Here we define that the tracker reaches its steady-state conditions in the state of rest or uniform motion characterized with 1g acceleration caused by gravity. Tilt angles are then calculated from three orthogonal acceleration components as:

$$a = \sqrt{a_x^2 + a_y^2 + a_z^2} \approx g \; ; \tag{1}$$

$$\theta = \sin^{-1}\left(\frac{a_x}{g}\right); \; \phi = \sin^{-1}\left(\frac{a_y}{g \cdot \cos\theta}\right) \tag{2}$$

where $\begin{bmatrix} a_x & a_y & a_z \end{bmatrix}^T$ is the gravity vector measured in the body frame. $\theta$ and $\phi$ are pitch and roll angles in the global frame.

For the magnetometer sitting in the horizontal plane, the yaw angle $\psi$ (also known as heading or azimuth angle) is always computed as:

$$\psi = \tan^{-1}\left(\frac{b_Y}{b_X}\right) \tag{3}$$

where $\begin{bmatrix} b_X & b_Y & b_Z \end{bmatrix}^T$ is the geomagnetic vector measured in the horizontal frame. In order to calculate the yaw angle at any position, the magnetometer orientation needs to be mathematically rotated to the horizontal plane through a transformation matrix (see Fig. 3):

$$\begin{bmatrix} b_X \\ b_Z \end{bmatrix} = \begin{bmatrix} \cos(-\theta) & -\sin(-\theta) \\ \sin(-\theta) & \cos(-\theta) \end{bmatrix} \begin{bmatrix} b_{x'} \\ b_{z'} \end{bmatrix} = \begin{bmatrix} \cos\theta & \sin\theta \\ -\sin\theta & \cos\theta \end{bmatrix} \begin{bmatrix} b_{x'} \\ b_{z'} \end{bmatrix}; \tag{4}$$

$$\begin{bmatrix} b_{y'} \\ b_{z'} \end{bmatrix} = \begin{bmatrix} \cos\phi & -\sin\phi \\ \sin\phi & \cos\phi \end{bmatrix} \begin{bmatrix} b_y \\ b_z \end{bmatrix}; \tag{5}$$

by substituting (5), (4) can be rewritten as:

$$\begin{bmatrix} b_X \\ b_Y \\ b_Z \end{bmatrix} = \begin{bmatrix} \cos\theta & \sin\theta\sin\phi & \sin\theta\cos\phi \\ 0 & \cos\phi & -\sin\phi \\ -\sin\theta & \cos\theta\sin\phi & \cos\theta\cos\phi \end{bmatrix} \begin{bmatrix} b_x \\ b_y \\ b_z \end{bmatrix} \tag{6}$$

where $\begin{bmatrix} b_X & b_Y & b_Z \end{bmatrix}^T$, $\begin{bmatrix} b_x & b_y & b_z \end{bmatrix}^T$, and $\begin{bmatrix} b_{x'} & b_{y'} & b_{z'} \end{bmatrix}^T$ denote the magnetic vector measured in the local frame, the global frame, and the coordinate axis in between them, respectively.

Now at any steady-state position, the sensor's tilt-compensated heading (yaw angle) can be computed from (3) and (6). There are two points need to be clarified before we move to the next stage:

1) The above algorithm is only valid under the steady-state assumption. Any acceleration, except for the acceleration caused by the earth gravity field, will affect the accuracy of tilt angles and consequently result in heading errors. If the tilt error, or uncertainty, is allowed to be ±0.5º, then the acceleration tolerance should be set as sin(±0.5º), or ±1%. In other words, the motion tracker can be assumed at its steady-state position if the acceleration measured is within this range.

2) Considering the limits in the $\tan^{-1}$ function, the heading calculations must account for the sign of the magnetometer readings and the values on four quadrant boundaries.

Next, angular rates are computed from regulated voltages as:

$$\omega = \left(V_{out} - V_{off}\right) \cdot \frac{\Delta\omega}{\Delta V} \tag{7}$$

where $\omega$ is the angular velocity. $V_{out}$ and $V_{off}$ represent the sensor's output and 0 rad/s offset voltage, respectively. $\frac{\Delta\omega}{\Delta V}$ denotes the sensitivity of the gyroscope. The angular position of the sensor, $\theta$, is calculated by integrating of the angular velocity over time $t$:

$$\theta(t) = \int \omega(t')dt' \, . \tag{8}$$

Every time the sensor unit reaches a steady-state position, errors caused by drift and scale factor of the gyroscope are continuously corrected based upon the difference between the integration results and the calculation results from accelerometer-magnetometer measurements. Such a close loop system is able to achieve high accuracy for both static and dynamic measurements.

Finally, the earth's gravity is filtered out from the direct measurement of the accelerometer. And the new acceleration vector is now able to be transferred into the global coordinate through a transformation matrix similar to (6). In total, the sensor unit provides 6 DOF information of the subject, including orientation, tri-axis angular velocity, and position integrated from acceleration.

## IV. ERROR ANALYSIS AND ELIMINATION

Our goal is to implement a low-cost inertial/magnetic tracker based on commercially available sensors and to satisfy a requirement of less than ±1º accuracy in orientation determination. Preliminary tests are performed to understand

the physical parameters of individual sensors, such as scale factor, bias, noise characteristics, linearity, sensitivity, ADC resolution, etc. Elimination methods are then verified on an experimental setup made of two orthogonal precision rotary stages with a resolution of 0.1º. The following parts are organized into four sections: the first three parts discuss component-level error cancelling methods for the accelerometer, magnetometer, and gyroscope sensors; the last section takes into account common disturbances and system-level error factors including temperature changes and sensor misalignments.

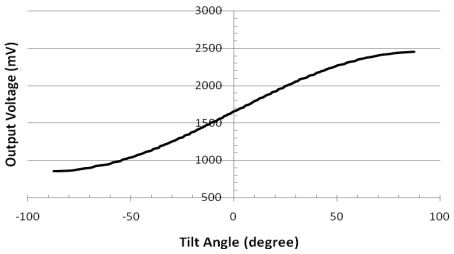


Fig. 4. Nonlinear relationship output of x-axis accelerometer.

### A. Accelerometer

Accelerometer error in measuring tilt angles arises from scale factor, nonlinearity, output drifts, and misalignment [10]. The last two will be discussed in section D since they are shared by all modules in the sensor unit.

Scale factor (SF, units: V/g), or sensitivity, is defined as the ratio of a change in the output to a change of the input intended to be measured. Bias (B, units: V), or zero offset, is the average output of the sensor over a time measured at specified operating conditions that has no correlation with the input. According to the manufacturer's specification sheets, scale factor, SF, bias, B, and acceleration, $a$ (units: g) are determined as:

$$SF = \frac{V_{+g} - V_{-g}}{2};\ B = \frac{V_{+g} + V_{-g}}{2}; \tag{9}$$

$$a = \frac{V_{out} - B}{SF} \tag{10}$$

where $V_{+g}$, $V_{-g}$, and $V_{out}$ are the output voltages when the sensor is aligned with, aligned opposite to the direction of gravity, and at any tilt angle, respectively. With the acceleration measured from (10), tilt angles at any stead-state position can be calculated from (2).

The nonlinear relationship between tilt angles and output voltages is a result of the construction of the sensor. A MEMS-based capacitive accelerometer normally consists of fixed fingers attached to the base and moving fingers attached to a center mass supported by suspension springs. Any tilt of the sensor leads to the change of the capacitance proportional to the overlapping area and distance between the moving and fixed fingers [10]. Therefore, the principle of the sensor gives it a sinusoidal input vs. output relationship.

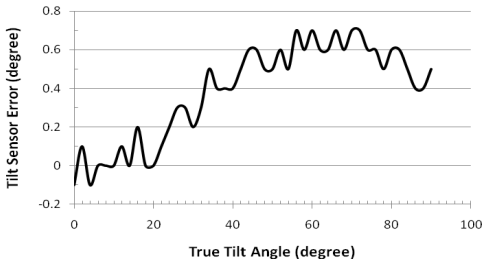


Fig. 5. Tilt errors due to the nonlinear characteristics of the accelerometer (average error: 0.38º).

A simple experiment is performed to reveal the nonlinear behavior of the MMA7260Q accelerometer (see Fig. 4). The slope of the curve indicates the sensitivity of the device: as the tilt angle increases from $0^\circ$ towards $90^\circ$, the sensitivity decreases. Because of this nonlinearity, the resolution of the ADC needs to be determined at $0^\circ$ and $90^\circ$ to ensure the lowest resolution is still within the requirement. Therefore, taking the accelerometer readings at 0g (0º tilt for one axis) and 1g (90º tilt), an ADC would result in the following resolutions:

$$SV = \frac{10^3 n}{2^m}; \tag{11}$$

$$RES_0 = \sin^{-1}\left(\frac{SV}{SF}\right); \tag{12}$$

$$RES_{90} = 90^\circ - \sin^{-1}\left(\frac{SF \cdot g - SV}{SF \cdot g}\right) \tag{13}$$

where $SV$ (units: mV) is the step voltage rounded off to one decimal as an $m$-bit ADC cuts $n$ V supply into $2^m$ steps. $RES_0$ and $RES_{90}$ (units: degree) are the resolutions at 0g and 1g, respectively. For example, if the MMA7260Q with a 10-bit ADC running on a 3.3V power, the system provides a 0.23º resolution at the highest sensitivity point and a 5.13º resolution at the lowest sensitivity point. An 11-bit ADC gives a range of resolution from 0.11º to 3.62º. An experiment on the LIS3LV02DQ accelerometer with 12/16 bit data representation (11-bit ADC) verifies the above analysis (see Fig. 5). Due to the nonlinearity of the accelerometer, it is more accurate when the sensing axis is closer to 0º, and less sensitive when closer to 90º. However, errors at the higher end do not exceed the estimation value because errors are reduced by a low-pass filter and the calculation algorithm, which takes average measurements over time. In such a way, an overall average error less than ±0.5º in tilt angle measurement is secured.

### B. Magnetometer

Heading accuracy is affected by magnetic sensor errors, ADC resolution, platform tilt errors, geomagnetic variation, and nearby ferrous distortions [12]. Of these errors, the last

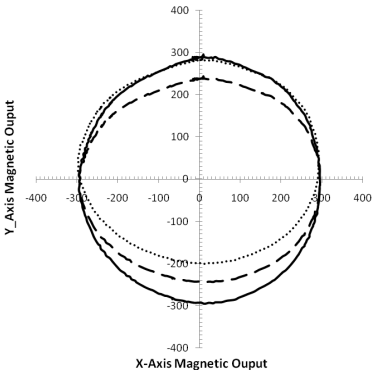


Fig. 6. Output of the MicroMag3 magnetometer (relative magnetic field values, range from -32768 to 32768; raw data, dotted line; after cancelling hard-iron distortions, dashed line; after gain matching, solid line).

one is addressed and discussed below. Nearby ferrous distortions are mainly caused by hard-iron and soft-iron. Hard-iron distortions are caused by permanent magnets and magnetized object at fixed location and within close proximity to the sensors. Figure 6 (dotted line) shows the result of an experiment where the magnetometer measures a biased field; a constant magnetic component is added along each axis of sensor output; and the center point of the circle shifts. Soft-iron distortions are the result of interactions between the earth's magnetic field and any magnetically "soft" material within close proximity to the sensors. In technical terms, soft materials have a high permeability–a measure of how well it serves as a path for magnetic lines of force. According to their characteristics, heading errors are written as a function of nearby ferrous distortions:

$$\begin{aligned} E(\psi_m) &= E_H(\psi_m) + E_S(\psi_m) \\ &= R_H \sin\left(\psi_m + \delta_H\right) + R_S \sin\left(2\psi_m + \delta_S\right) \end{aligned} \tag{14}$$

where $E_H$ and $E_S$ are errors caused by hard-iron and soft-iron distortions, respectively. $R_H$, $R_S$, $\delta_H$, and $\delta_S$ are the hard-iron and soft-iron error signal amplitudes and phase shifts, respectively. Although there are various methods to reduce soft-iron distortions, it is more straightforward to remove any soft iron materials near the sensor and eliminate the hard-iron effects through the following two steps:

$$offset = \frac{b_{\max} + b_{\min}}{2}; \tag{15}$$

$$range = b_{\max} - b_{\min}; \tag{16}$$

Subtraction: $$b_t = b_m - offset; \tag{17}$$

Gain matching:

$$\text{if } range_x > range_y,\ b_{t_y} = b_{t_y} \cdot \frac{range_x}{range_y};$$

$$\text{if } range_x < range_y,\ b_{t_x} = b_{t_x} \cdot \frac{range_y}{range_x} \tag{18}$$

where vectors $b_t$, $b_m$, $b_{\max}$, and $b_{\min}$ are the true magnetic field value, measurement value, maximum, and minimum readings along the three axis, respectively. $b_m$, $b_{\max}$, and $b_{\min}$ are recorded during the multi-point calibration in which the magnetometer is mounted horizontally and rotated two cycles for about 720º. As shown in Fig. 6, the output plot of X vs. Y forms a perfect circle centered at the origin after the two-step compensation. This successfully gets rid of heading errors caused by nearby hard-iron distortions.

Platform tilt is another major source that contributes to heading errors. Experimental results (see Fig. 7) show that the method aforementioned in section III significantly reduces this type of error to within ±1º.

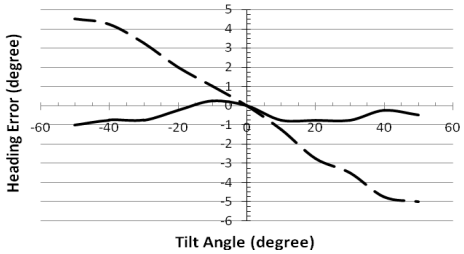


Fig. 7. Heading errors when tilt angles between ±50º (heading errors before compensation, dashed line; after compensation, solid line).

### C. Gyroscope

Major error sources of a rate gyroscope include its ADC resolution, temperature drifts, electromagnetic interference, scale factor, bias, etc. Scale factor and bias are considered for the scope of this section.

The transformation between the angular rate measured by the gyroscope and its global representative is given as [13]:

$$r = \frac{\sin\phi}{\cos\theta}\omega_y + \frac{\cos\phi}{\cos\theta}\omega_z \tag{19}$$

where r is the yaw rate. $\omega_y$ and $\omega_z$ are the body-fixed y-axis and z-axis angular rate, respectively. The measured angular rate, $\omega_m$, is a function of the true angular rate, $\omega_t$, scale factor, SF, and bias, B:

$$\omega_m = (1 + SF)\omega_t + B. \tag{20}$$

In a simplified model when $\phi \approx 0$, the yaw angular position at the discrete time (t+n), $\omega_t(t+n)$ is written as:

$$\psi_t(t+n) = \psi_t(t) + \frac{1}{1+SF}\sum_{i=t}^{t+n-1}\frac{\cos\phi(i)}{\cos\theta(i)}\omega_{m_z}(i) - \frac{B}{1+SF}\sum_{i=t}^{t+n-1}\frac{\cos\phi(i)}{\cos\theta(i)} \quad (21)$$

Therefore, with a number of true positions from the tilt-compensated magnetometer readings and measurements from the rate gyroscope over a short period, the least squares algorithm can be used to estimate scale factor and bias values by solving the matrix equation stacking from (21). With these calibration coefficients, a continuous compensation then becomes possible for position error correction. As shown in Fig. 1, the three sensor modules construct a typical feedback loop, which can reduce the error propagation during the integration of gyroscope measurements.

### *D. Common Disturbances and System-level Errors*

Temperature effects and misalignment errors are discussed in this section. Manufactures' datasheets show that scale factor and bias are sensitive to temperature change. Although we can make an assumption of constant environmental temperature, the gradual heating up of the sensor circuitry is still out of our control. The experimental result performed on the LIS3LV02DQ accelerometer and MicroMag3 magnetometer at room temperature (25ºC) shows that they can reach their steady state within one minute and their readings remain approximately constant over time. The differences between the initial and steady-state values are less than 2‰ for the accelerometer and less than 0.5% for the magnetometer. Thus, temperature effects do not have significant effects on bias and scale factor at room temperature. There are two reasons to explain the phenomenon: circuitry temperatures do not change much during the operation; and sensors already have certain built-in temperature compensation mechanisms. For applications requiring a higher accuracy, the user can either use extended Kalman filtering [14] or correct errors with a pre-stored error lookup table in the MCU. Environmental temperature can be measured with the internal thermometer in the ADXRS300 gyroscope.

Misalignment errors occur at both the sensor level and the system level. Errors at the sensor level are normally compensated by the manufactures through their on-chip error tables. At the system level, misalignment of individual sensor with respect to the global frame simply results in a constant error. To eliminate system-level misalignment errors, we choose to build the tracker using surface-mount technology (SMT) components, and measure the current mounting declination before the calibration.

## V. CONCLUSION

This paper discusses the design, implementation and error elimination methods for an inertial/magnetic motion tracker using a combination of accelerometer, magnetometer, and rate gyroscopes. The sensor has several advantages in terms of its compact size, low cost, and high accuracy in orientation measurement. Having acknowledged the behavior and characteristics of individual components via a series of tests, we propose sensor calibration and error cancelling methods for the prototype. Preliminary tests prove that it achieves ±1º accuracy in orientation measurement for low-g motion sensing applications. However, supplemental tests still need to be performed for motion capture applications under high dynamic conditions. Future work will also include employing the motion tracker in various applications, such as biomechanics, indoor navigation, etc.

## REFERENCES


[1] G. Welch, E. Foxlin, "Motion Tracking: No Silver Bullet, but a Respectable Arsenal," *IEEE Computer Graphics and Applications*, Vol. 22, No. 6, pp. 24-38, 2002.

[2] B. S. Davis, 'Using Low-Cost MEMS Accelerometers and Gyroscopes as Strapdown IMUs on Rolling Projectiles," *Proc: Position Location and Navigation Symp.*, pp. 594-601, Apr. 1998.

[3] A. T. M. Willemsen, J. A. Van Alste, and H. B. K. Boom, "Real-time Gait Assessment Utilizing a New Way of Accelerometry," *J. Biomech.*, vol. 23, no. 8 (1990), pp. 859-863.

[4] J. R. W. Morris, "Accelerometery – a Technique for the Measurement of Human Body Movements," *J. Biomech.*, vol. 6, no. 7 (1973), pp. 29-36.

[5] K. Aminian, C. Trevisan, B. Najafi, H. Dejnabadi, C. Frigo, E. Pavan, A. Telonio, F. Cerati, E. C. Marinoni, P. Robort, and P.-F. Leyvraz, "Evaluation of an Ambulatory System for Gait Analysis in Hip Osteoarthritis and After Total Hip Replacement," *Gait & Posture*, vol. 20 (2004), pp. 102-107.

[6] H. J. Luinge, and P. H. Veltink, "Measuring Orientation of Human Body Segments Using Miniature Gyroscope and Accelerometers," *Med. Biol. Eng. Comput.*, vol. 43 (2005), pp. 273-282.

[7] E. Bachmann, I. Duman, U. Usta, R. McGhee, X. Yun, and M. Zyda, "Orientation tracking for humans and robots using inertial sensors," in *Proc. Int. Symp. Computational Intelligence in Robotics and Automation (CIRA)*, 1999, pp. 187–194.

[8] E. R. Bachmann, X. Yun, D. McKinney, R. B. McGhee, M. J. Zyda, "Design and Implementation of MARG Sensors for 3-DOF Orientation Measurement of Rigid Bodies," *Proc. of the 2003 IEEE Intl. Conf. on Robotics and Automation (ICRA)*, Taipei, Taiwan, Sept 2003, pp. 14-19.

[9] R. Zhu and Z. Y. Zhou, "A Real-Time Articulated Human Motion Tracking Using Tri-Axis Inertial/Magnetic Sensors Package," *IEEE Trans. on Neural Systems and Rehabilitation Engineering*, Vol. 12, No. 2, 2004.

[10] W. T. Ang, S. Y. Khoo, P. K. Khosla, and C. N. Riviere, "Physical Model of a MEMS Accelerometer for Low-g Motion Tracking Applications," *Proceedings of the 2004 IEEE Intl. Conference on Robotics & Automation*, New Orleans, LA, USA, April 2004, pp. 1345-1351.

[11] M. Horton, C. Kitchin, "A Dual Axis Tilt Sensor Based on Micromachined Accelerometers," *Sensors*, April 1996.

[12] M. J. Caruso, "Applications of Magnetic Sensors for Low Cost Compass Systems," *IEEE Symp. Position Location and Navigation*, San Diego, CA, USA, 2000, pp.177-184.

[13] D. H. Titterton, J. L. Weston, *Strapdown inertial navigation technology (2nd ed.)*, Institution of Electrical Engineers, United Kingdom, 2004.

[14] B. Barshan, H. F. Durrant-Whyte, Inertial Navigation Systems for Mobile Robots, *IEEE Trans. On Robotics and Automation*, Vol. 11, No. 3, June 1995, pp. 328-342.